Solution Studies and Structural Model of the Extracellular Domain of the Human Amyloid Precursor Protein

Matthias Gralle,* Michelle M. Botelho,* Cristiano L. P. de Oliveira,† Iris Torriani,†‡ and Sérgio T. Ferreira*‡
*Department of Medical Biochemistry, Federal University of Rio de Janeiro, Rio de Janeiro RJ 21944-590, Brazil; †Instituto de Física "Gleb Wataghin," Unicamp, Campinas SP 13084-971, Brazil; and ‡Laboratório Nacional de Luz Síncrotron (LNLS), Campinas SP 13084-9701, Brazil

ABSTRACT The amyloid precursor protein (APP) is the precursor of the β-amyloid peptide (Aβ), which is centrally related to the genesis of Alzheimer's disease (AD). In addition, APP has been suggested to mediate and/or participate in events that lead to neuronal degeneration in AD. Despite the fact that various aspects of the cell biology of APP have been investigated, little information on the structure of this protein is available. In this work, the solution structure of the soluble extracellular domain of APP (sAPP, composing 89% of the amino acid residues of the whole protein) has been investigated through a combination of size-exclusion chromatography, circular dichroism, and synchrotron radiation small-angle x-ray scattering (SAXS) studies. sAPP is monomeric in solution (65 kDa obtained from SAXS measurements) and exhibits an anisometric molecular shape, with a Stokes radius of 39 or 51 Å calculated from SAXS or chromatographic data, respectively. The radius of gyration and the maximum molecular length obtained by SAXS were 38 Å and 130 Å, respectively. Analysis of SAXS data further allowed building a structural model for sAPP in solution. Circular dichroism data and secondary structure predictions based on the amino acid sequence of APP suggested that a significant fraction of APP (30% of the amino acid residues) is not involved in standard secondary structure elements, which may explain the elongated shape of the molecule recovered in our structural model. Possible implications of the structure of APP in ligand binding and molecular recognition events involved in the biological functions of this protein are discussed.

INTRODUCTION

The amyloid precursor protein (APP) is genetically and biochemically linked to the genesis of Alzheimer's disease (AD), the most widespread cause of dementia in industrialized countries (De Strooper and Annaert, 2000). Human APP is a ubiquitous transmembrane protein that spans the plasma membrane a single time (Kang et al., 1987) and exists in various alternatively spliced isoforms. The predominant non-neuronal isoforms, APP_{751} and APP_{770}, contain a Kunitz-type protease inhibitor domain (Kitaguchi et al., 1988; Ponte et al., 1988; Tanzi et al., 1988; see Fig. 1). This domain has been shown to be a modulator of the blood-clotting cascade (Van Nostrand et al., 1990). The predominant isoform in neurons, APP_{695}, is a moderately glycosylated isoform lacking the protease inhibitor domain (De Strooper and Annaert, 2000). On its way to the plasma membrane, APP undergoes (N + O)-glycosylation, tyrosine-sulfation (Weidemann et al., 1989), and phosphorylation (Caporaso et al., 1992).

The half-life of APP in the plasma membrane is <10 min (Koo et al., 1996). It is either cleaved extracellularly or recycled to an intracellular compartment, apparently acidic endosomal vesicles and lysosomes. Proteolytic cleavage of APP can also occur intracellularly, resulting in a pool of secreted APP (sAPP) contained in vesicles that are subject to polarized traffic (Haass et al., 1994). Extracellular cleavage of APP occurs predominantly by action of α-secretase (Lammich et al., 1999), which cleaves APP at a site located 13 amino acid residues upstream from its membrane insertion (Fig. 1). APP can also be cleaved by β-secretase at the β-site, located 29 amino acid residues upstream from its membrane insertion point (Hussain et al., 1999; Sinha et al., 1999; Vassar et al., 1999; Yan et al., 1999; Lin et al., 1999). The soluble extracellular fragments released upon cleavage by both α-secretase(s) (sAPPα) and β-secretase (sAPPβ) can be detected in the extracellular medium (Seubert et al., 1993). Further intramembranous cleavage by γ-secretase(s) (Durkin et al., 1999) releases either p3 or the β-amyloid peptide, Aβ, to intracellular vesicles or the extracellular medium, and leaves a cytoplasmic stub that can migrate to the nucleus and modulate gene expression (Kimberly et al., 2001; Gao and Pimplikar, 2001; Fig. 1). Aβ can aggregate in the extracellular medium to form amyloid fibrils and the senile plaques characteristically found in AD brains and thought to be implicated in neuronal death in this disease (Masters et al., 1985).

Research into the biochemistry and cell biology of neuronal dysfunction and death in AD has mainly focused on Aβ. However, considerable evidence indicates that other domains of APP may be important for normal neuronal function (Sisodia and Gallagher, 1998) and may also be involved in the neuropathology of AD (Barger and Harmon, 1997). Although several studies have concentrated on the cell biology of APP, it has not yet been possible to fully understand how the in vitro biochemical properties of this protein relate to its functions in a

Submitted January 5, 2002, and accepted for publication July 16, 2002.
Address reprint requests to Sérgio T. Ferreira, Cidade Universitaria, Rio de Janeiro RJ 21941-590, Brazil. Tel.: 55-21-270-5988; Fax: 55-21-270-8647; E-mail: ferreira@bioqmed.ufrj.br.

0006-3495/02/12/3513/12 $2.00

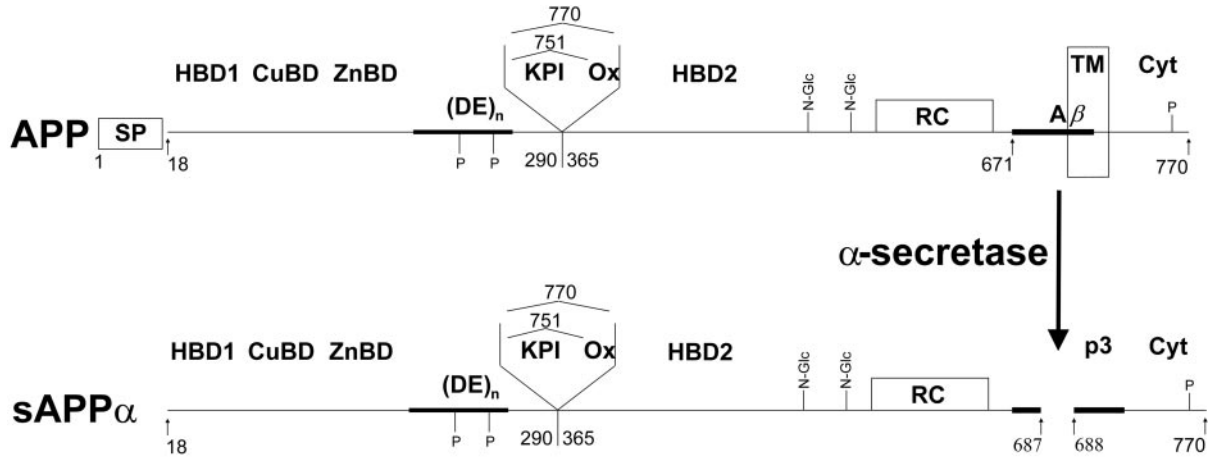

FIGURE 1 Domain structure and cleavage of APP. *APP:* the entire transmembrane protein, including the signal peptide (*SP*), numbered as in APP_{770}. The 56-residue *KPI* domain (1AAP.PDB, Hynes et al., 1990), which is present in APP_{751} and APP_{770}, and the 19-residue Ox2 sequence (*Ox*), which is present in APP_{770}, are shown above their insertion sites. *HBD1, HBD2:* putative heparin-binding domains (HBD1 is equivalent to 1MWP.PDB, Rossjohn et al., 1999). *CuBD:* copper-binding domain. *ZnBD:* putative zinc-binding domain. $(DE)_n$: Asp- and Glu-rich region with two Tyr-phosphorylation (*P*) sites. *N-Glc: N*-glycosylation sites. *RC:* predicted random coil region. *TM:* transmembrane domain. *Aβ:* amyloidogenic sequence that reaches partially into the transmembrane domain. Cleavage by β-secretase at its N-terminus and γ-secretase at its C-terminus (not shown) gives rise to the Aβ peptide. *Cyt:* cytoplasmic domain of APP with a Tyr-phosphorylation site (*P*). Cleavage by α-secretase releases the soluble *sAPPα* fragment (numbered as in $sAPP\alpha_{770}$), carrying at its C-terminus part of the amyloidogenic sequence (*bold*). The membrane-bound C-terminal stub can be further cleaved by γ-secretase (not shown) into the *p3* peptide (*bold*) and the cytoplasmic domain (*Cyt*). The diagram shows that $sAPP\alpha_{770}$ is equivalent to APP18–687 (670 amino acid residues), while $sAPP\alpha_{751}$ has 651 residues, and $sAPP\alpha_{695}$ has 595 residues.

cellular context (Van Nostrand et al., 1990; Multhaup et al., 1996). Furthermore, few structural data on APP are currently available. This clearly represents an obstacle to understanding structure-function relationships of APP and the events leading to its pathological proteolysis and secretion.

The structure of the Kunitz-type protease inhibitor domain present in the major non-neuronal isoforms of APP has been obtained by x-ray crystallography (Hynes et al., 1990). Another fragment of known structure is the N-terminal domain (Rossjohn et al., 1999; indicated as HBD1 in Fig. 1), which shows a general similarity to other proteoglycan receptors. It has been proposed that the N-terminal domain contains one of several binding sites for heparan sulfate proteoglycans (Mok et al., 1997) and mediates their effects on cell viability and growth. The N-terminal domain is also thought to bind to fibulin-1 (Ohsawa et al., 2001). Other known ligands of APP are zinc and copper ions, which appear to bind to the cysteine-rich region near the N-terminal domain (Bush et al., 1994; Hesse et al., 1994; Fig. 1), and collagen and laminin, which are thought to bind to the glycosylation domain (Beher et al., 1996; Narindrasorasak et al., 1992).

The soluble ectodomain of APP (sAPP) is much more amenable to physicochemical studies (e.g., using spectroscopic and chromatographic techniques) than the intact transmembrane protein, and appears to mediate similar physiological roles (Saitoh et al., 1989; Breen et al., 1991; Mattson et al., 1993). In the present work, we have expressed recombinant sAPPα isoforms in the methanolotrophic yeast *Pichia pastoris* (Henry et al., 1997). The proteins were purified to homogeneity and their conformations were analyzed by size-exclusion chromatography (SEC), circular dichroism (CD), and small-angle x-ray scattering (SAXS). SAXS is a well-established technique for obtaining structural information on macromolecules in solution under close to physiological conditions (Trewhella, 1997). Over the past few years, the use of synchrotron radiation and new theoretical approaches have provided solution structural data at better than 1.5 nm resolution using SAXS (Chacón et al., 1998; Svergun, 1999, 2001). The results obtained with sAPPα show an elongated shape for the molecule, and are discussed in terms of possible structural correlations with biological functions of the extracellular domain.

MATERIALS AND METHODS

Protein expression

The three strains of *Pichia pastoris* expressing $sAPP\alpha_{695}$, $sAPP\alpha_{751}$, and $sAPP\alpha_{770}$ (see Fig. 1) were kindly provided by Dr. R. Cappai (University of Melbourne, Australia) and were grown at 30°C in YPD [1% (w/v) yeast extract (Gibco, Carlsbad, CA), 2% (w/v) peptone (Gibco), 2% (w/v) D-glucose (Sigma, St. Louis, MO)]. Expression of each of the recombinant protein isoforms was induced during 48 h in BMMY [1% (w/v) yeast extract, 2% (w/v) peptone, 1.34% (w/v) yeast nitrogen base without amino acids (Sigma), $4 \cdot 10^{-5}$ % biotin (Sigma), 2% methanol (Merck, Darmstadt, Germany)] (Henry et al., 1997).

Purification of sAPP

Purification was carried out using a modification of the method of Henry et al. (1997). Yeast cultures (0.5–2 l) were centrifuged at 16.000 × *g* for 10 min at 4°C and the supernatants were filtered (0.45 μm, Whatman, Springfield Mill, U.K.). From this point the protein was always kept on ice. The supernatant was diluted with buffer A [20 mM imidazole, 5 mM EDTA, 10 mg/l phenylmethylsulfonyl fluoride (PMSF), pH 5.5] to ionic strength 0.2 and applied at a flow-rate of 7 ml/min onto a Q-Sepharose column (HR 26–10, Pharmacia, Uppsala, Sweden) pre-equilibrated with 6 vol of buffer A. The column was washed with 20 vol of buffer B (buffer A + 250 mM NaCl) and the protein was eluted in 2-ml fractions of buffer C (20 mM Tris-HCl, 1 M NaCl, 5 mM EDTA, 10 mg/l PMSF, pH 7.4). Fractions with high absorption at 280 nm were pooled and desalted in pre-packed Sephadex G-25 columns (Pharmacia). The desalted pool was applied onto a 5-ml HiTrap heparin Sepharose column (Pharmacia) connected to an HPLC system and pre-equilibrated with 50 mM Tris-HCl, pH 7.4. The column was washed until A_{280} had reached baseline, and the protein was then eluted with a linear gradient of salt up to 1 M NaCl. Eluted peaks were monitored by A_{280}. The fractions in the sAPP peak were pooled and desalted in 50 mM Tris-HCl, pH 7.4, concentrated using a Centricon-30 device (Amicon, Bedford, MA), and stored at 4°C. Aliquots from the conditioned medium and all subsequent purification steps were analyzed by SDS-PAGE (Laemmli, 1970), and the identity of sAPP was verified by Western blots using anti-APP monoclonal antibody 22C11 (Boehringer Mannheim, Mannheim, Germany).

Protein determination

The protein contents of purified and desalted sAPP samples were calculated using $\epsilon_{280\ nm} = 60{,}110\ M^{-1}\ cm^{-1}$ for sAPPα_{695} and $\epsilon_{280\ nm} = 70{,}455\ M^{-1}\ cm^{-1}$ for sAPPα_{751} and sAPPα_{770}. These coefficients were calculated by adding up the extinctions of all tryptophan, tyrosine, and cystine residues in sAPP ($\epsilon_{Trp} = 5500\ M^{-1}\ cm^{-1}$, $\epsilon_{Tyr} = 1490\ M^{-1}\ cm^{-1}$, and $\epsilon_{Cys\text{-}Cys} = 125\ M^{-1}\ cm^{-1}$; Pace et al., 1995). sAPPα_{695} has 7 Trp, 14 Tyr, and 12 Cys residues, whereas sAPPα_{751} and sAPPα_{770} have 8 Trp, 17 Tyr, and 18 Cys residues.

Copper-reducing activity assay

Variable amounts of sAPP were diluted to 700 μl in a solution containing 750 μM neocuproin and 100 μM $CuCl_2$. sAPP samples and negative controls not containing protein were incubated for 60 min at 37°C, and absorption spectra were measured at regular time intervals. In the wavelength region from 400 to 500 nm, the spectra of all sAPP-containing samples contained a single peak at 454 nm. The concentration of reduced copper ions was calculated from the absorption at 454 nm using the absorption coefficient of the neocuproin-Cu(I) complex at 454 nm ($\epsilon_{454} = 7200\ M^{-1}\ cm^{-1}$; Proudfoot et al., 1997).

Circular dichroism

sAPPα isoforms were diluted to a concentration of 0.1 mg/ml in 50 mM Tris-Cl, pH 7.4. Spectra were measured on Jasco J-715 and J-810 spectropolarimeters (pathlength 0.1 or 0.2 cm). Secondary structure contents were calculated from CD data using the programs CONTINLL, SELCON3, and CDSSTR contained in the CDPro package (Sreerama and Woody, 2000). This package allows evaluation of the robustness of the analysis by comparing the values obtained using the three different algorithms, which use the same database of proteins with known three-dimensional structure.

Secondary structure prediction

The amino acid sequence of sAPPα_{770} was analyzed to predict possible secondary structure elements using the programs NNPREDICT (Kneller et al., 1990) and DPM, DSC, GOR4, HHNC, MLRC, PHD, Predator, SIMPA96, and SOPM included in the NPS@ package (Combet et al., 2000).

Size-exclusion chromatography

This was performed on a GPC-100 column (250 × 4.6 mm, 15,900 theoretical plates, Eichrom Technologies, Inc., Darien, IL) connected to an HPLC apparatus (Shimadzu, Kyoto, Japan). GPC-100 is a silica-based column and, according to manufacturer's instructions, may only be used at pH ≤ 7. The column was equilibrated and operated at 22°C in buffer containing 50 mM Tris, 150 mM NaCl, pH 6.8. The sample volume was 100 μl and the flow rate was 0.3 ml/min. Elution was monitored by absorbance at 280 nm. The void volume retention time, t_0, was 5.25 min (measured by the elution of plasmid DNA) and the total volume retention time, t_T, was 11.17 min (measured by the elution of Trp-Gly-Gly). From these values, the partition coefficient of a given protein, K_d, was calculated as:

$$K_d = (t_e - t_0)/(t_T - t_0) \quad (1)$$

t_e being the elution time of a given protein. The K_d values for four proteins of known Stokes radii (ovalbumin, 3.05 nm; bovine serum albumin, 3.55 nm; apoferritin, 6.1 nm; thyroglobulin, 8.5 nm; Pharmacia Biotech) were measured to construct the Porath plot according to the empirical relation (Siegel and Monty, 1966):

$$(K_d)^{1/3} = a \times r_{Stokes} + b \quad (2)$$

The Stokes radii of the three sAPPα isoforms were then estimated from the Porath plot by a linear least-squares fit. The concentrations of the three sAPPα isoforms varied between 0.06 μM and 3 μM in different chromatographic runs without any changes in elution time. Very similar results were obtained using a Laurent and Killander plot, according to the relation (Siegel and Monty, 1966):

$$(-\log K_d)^{1/2} = a \times r_{Stokes} + b \quad (3)$$

The uncertainties in known Stokes radii and the variation in our measured $(K_d)^{1/3}$ values are both of the order of 1%, while the goodness of the linear least-squares fit is given by $r^2 = 0.96$ for both Porath and Laurent and Killander plots.

SAXS measurements and data analysis

Small-angle x-ray scattering experiments were performed at the SAS beamline at the Laboratório Nacional de Luz Síncrotron (LNLS) in Campinas, Brazil (Kellermann et al., 1997). The monochromatic beam was tuned at 8.33 keV. The experimental setup included a temperature-controlled, 1-mm-thick sample cell with mica windows and a linear position-sensitive detector. Solutions of purified sAPPα_{695} used in the SAXS measurements had a maximum concentration of 2.6 mg/ml. The buffer solution used was 50 mM Tris, pH 7.4. The samples were kept at 10°C during the exposures. A second (more diluted) protein sample (1.3 mg/ml) was also measured to investigate possible concentration effects in the SAXS curves. Data acquisition was performed by taking ten 900-s frames for each sample, which allowed control of any possible radiation damage. Several sample-detector distances enabled detection in the q range accessible within the given experimental conditions: $0.02043\ Å^{-1} < q < 0.2997\ Å^{-1}$. Data treatment was performed using the software package TRAT-1D (Oliveira et al., 1997). Usual corrections for detector homogeneity, incident beam inten-

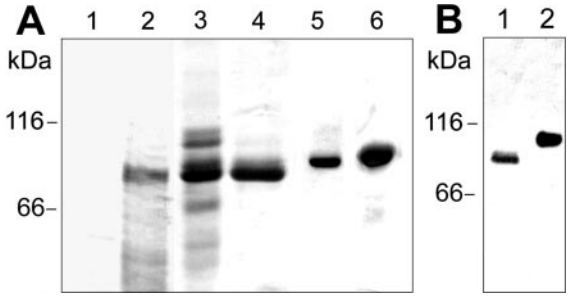

FIGURE 2 SDS-PAGE analysis of expressed and purified sAPPα isoforms. (*A*) The gel (7.0% acrylamide) was stained with Coomassie Brilliant Blue R. *Lane 1*: supernatant of yeast culture before induction; *lane 2*: supernatant of recombinant sAPPα_{695}-expressing yeast culture after induction; *lane 3:* pooled, desalted preparation of sAPPα_{695} after elution from the Q-Sepharose column; *lane 4*: purified sAPPα_{695} fraction eluted from the heparin-Sepharose column; *lane 5:* purified sAPPα_{751} fraction; *lane 6:* purified sAPPα_{770} fraction; 35 μl of sample were applied in lanes 1–3; 17.5 μl in lanes 5 and 6; 2 μl (3 μg of protein) were applied in lane 4 (this sample had been concentrated on Centricon-10). (*B*) Western blot of a 7.0% acrylamide gel. The antibody used was 22C11. *Lane 1:* purified sAPPα_{695}; *lane 2:* purified sAPPα_{770}.

sity, sample absorption, and blank subtraction were included in this routine. The output of this software provides the corrected intensities and error values. Data analysis was performed using GNOM (Svergun and Stuhrmann, 1991), SASHA (Svergun et al., 1996), DAMMIN (Svergun, 1999), and HYDRO (Garcia de la Torre, 1999) software packages.

RESULTS

Purification and expression of sAPPα

To obtain purified human sAPPα in the amounts required for biophysical measurements, recombinant isoforms sAPPα_{695}, sAPPα_{751}, and sAPPα_{770} were individually expressed in *Pichia pastoris*, which secreted sAPPα into the culture medium. SDS-PAGE analysis showed that, after induction, the conditioned medium contained a predominant protein band of the expected ~75 kDa for sAPP (Fig. 2 *A*, *lanes 1* and *2*). After the first purification step on an ion-exchange column, the protein-containing fractions were highly concentrated and enriched in sAPPα (Fig. 2 *A*, *lane 3*). From a heparin-affinity column, the peaks containing full-length sAPPα isoforms eluted at ~0.50 M NaCl, indicating a high affinity for heparin. Each of those peaks consisted of a single protein band (Fig. 2 *A*, *lanes 4–6*), which reacted strongly with anti-APP antibody in Western blots (Fig. 2 *B*, *lanes 1* and *2*).

Structural and functional integrity of recombinant sAPPα

Before proceeding with the structural characterization of sAPPα, it was important to ascertain that the purified recombinant proteins we used retained their expected biological activities. The expression system in *P. pastoris* was chosen because of the well-known ability of this eukaryote host to glycosylate and phosphorylate secreted proteins (Henry et al., 1997). *P. pastoris* has been reported to hyperglycosylate recombinant proteins less frequently than *Saccharomyces cerevisiae* does (Henry et al., 1997). The following lines of evidence indicated the structural and functional integrity of sAPPα. The high-affinity interaction between APP and heparin has been extensively investigated and associated with at least five different domains within sAPPα (Mok et al., 1997; Barger and Basile, 2001). Thus, the fact that recombinant sAPPα was strongly bound to heparin-Sepharose (Fig. 2 *A*, *lanes 4–6*) indicates structural preservation of the glycosaminoglycan-binding domains of APP. In addition, APP specifically catalyzes the reduction of copper (Multhaup et al., 1996), which is its only enzymatic activity known to date. This activity has been ascribed to a sequence in the N-terminal half of sAPPα (Multhaup et al., 1996; Fig. 1). We have investigated the capacity of the three purified sAPPα isoforms to catalyze the reduction of Cu(II) to Cu(I) using an assay based on the formation of a Cu(I)-neocuproin complex (Proudfoot et al., 1997). Upon incubation at 37°C, copper reduction catalyzed by APP was linear up to 60 min of incubation (Fig. 3 *A*), and the specific enzymatic rate thus calculated (0.24 mol Cu(I) formed per minute per mol sAPPα for all three isoforms) compares quite favorably to previously reported activities (Multhaup et al., 1996). Taken together, these results indicate that recombinant sAPPα retains the biological activities expected for genuine APP.

Circular dichroism

The far-UV CD spectra of the three sAPPα isoforms at 22°C (Fig. 3 *B*) were very similar to that reported for soluble APP directly purified from porcine brain (De La Fournière-Bessoueille et al., 1997) and did not exhibit significant changes in the temperature range between 10 and 30°C or between pH 6.8 and pH 7.4 (data not shown). Analysis of the CD spectra yielded a secondary structure content of 35–36% α-helix, 13–16% β-sheet, and 20–21% β-turn for the three sAPP isoforms, according to the three different algorithms implemented in the CDPro package (Sreerama and Woody, 2000). This indicates that a high percentage (30%) of the amino acid residues in sAPP are not involved in standard secondary structure elements in this protein.

Hydrodynamic radius of sAPP

Size-exclusion chromatography experiments revealed that the three isoforms of sAPPα eluted at the same elution volume under physiological buffer conditions (Fig. 4 *A*). The elution volume of sAPPα on a calibrated GPC-100 column corresponded to a Stokes radius of 51 Å (Fig. 4 *B*).

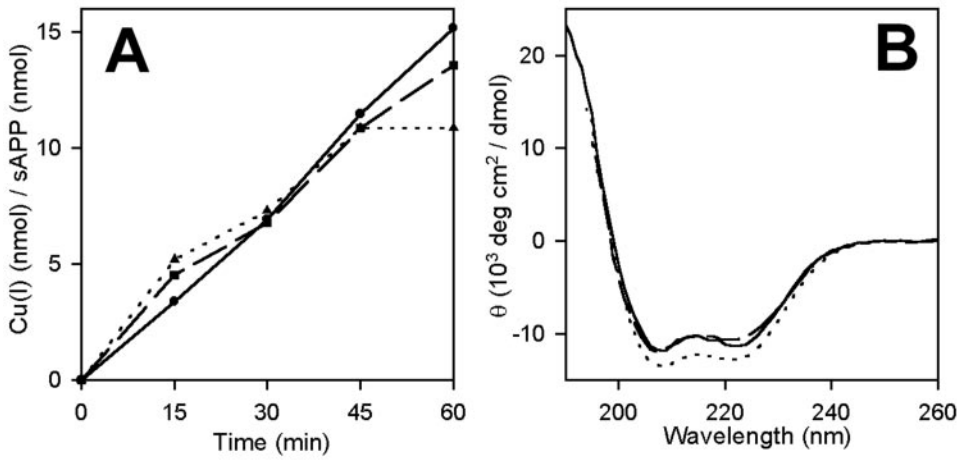

FIGURE 3 (*A*) Copper-reducing activity of sAPPα. Samples containing 100 μM $CuCl_2$, 750 μM neocuproin and various concentrations of sAPPα isoforms were incubated at 37°C and the concentration of Cu(I) as calculated from the absorption of the neocuproin-Cu(I) complex at 454 nm measured every 15 min. Buffer was 50 mM Tris-Cl, 50 mM NaCl, pH 7.4. *Circles and solid line:* sAPPα_{695}; *squares and broken line:* sAPPα_{751}; *triangles and dotted line:* sAPPα_{770}. (*B*) Circular dichroism spectra of sAPPα. sAPPα was diluted to 0.1 mg/ml in 50 mM Tris, pH 7.4. Circular dichroism was measured between 260 and 190 nm in 1 nm steps and the appropriate buffer signal was subtracted. *Solid line:* sAPPα_{695}; *broken line:* sAPPα_{751}; *dotted line:* sAPPα_{770}.

The elution profile of sAPPα_{751} presented a minor shoulder at lower elution volume, which could correspond to a small fraction of dimers or higher order oligomers in the sample.

SAXS measurements and data analysis

Small-angle x-ray scattering by sAPPα_{695} was measured using synchrotron radiation. The choice of this isoform is justified by the fact that it is predominant in neurons, and therefore of special interest in the elucidation of the pathogenesis of Alzheimer's disease. Furthermore, the secondary structure contents and the hydrodynamic radii of the three isoforms were shown to be the same within experimental error (see above), indicating that the three isoforms possess similar structures. The corrected experimental intensity data as a function of the modulus of the scattering vector q ($q = (4\pi/\lambda) \sin \theta$, where λ is the wavelength used and 2θ is the scattering angle) is shown in Fig. 5 *A*. A Guinier plot of the data (Guinier and Fournet, 1955) exhibited a linear region, indicating satisfactory monodispersity of the protein sample (Fig. 5 *A*, *inset*). The radius of gyration estimated using the Guinier approximation was R_g = 35 Å. There was no

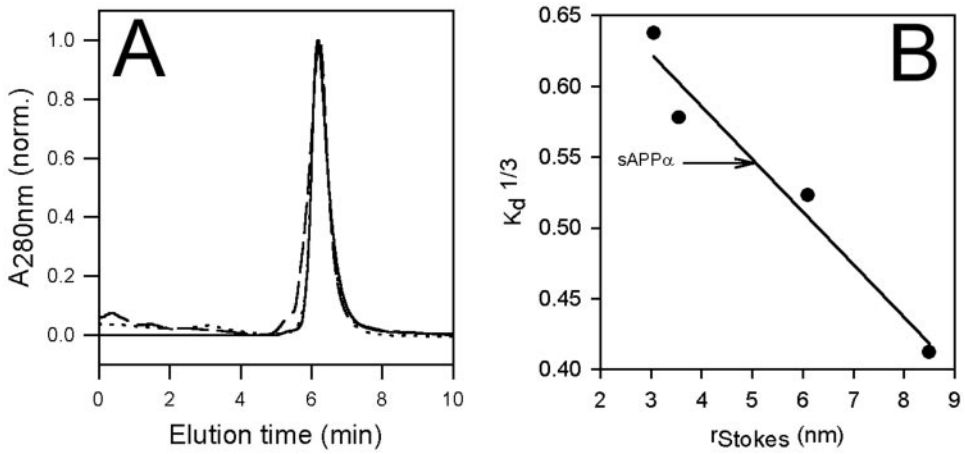

FIGURE 4 Size-exclusion chromatography of purified sAPP. (*A*) Elution profiles of sAPPα isoforms on a GPC-100 Gold column. Elution buffer: 50 mM Tris, 150 mM NaCl, pH 6.8. Flow rate: 0.3 ml/min. The void volume corresponded to 5.25 min (measured by the elution of plasmid DNA) and the total column volume corresponded to 11.17 min (measured by the elution of Trp-Gly-Gly). *Solid line:* sAPPα_{695}; *broken line:* sAPPα_{751}; *dotted line:* sAPPα_{770}. (*B*) Porath plot (Siegel and Monty, 1966) of reference proteins [from left to right, ovalbumin (45 kDa, 3.05 nm), bovine serum albumin (66 kDa, 3.55 nm), apoferritin (443 kDa, 6.1 nm), thyroglobulin (669 kDa, 8.5 nm)]. The cubic root of K_d is plotted against the Stokes radius of each protein. *Solid line*: linear least-squares fit. Arrow indicates the measured K_d for all three sAPPα isoforms.

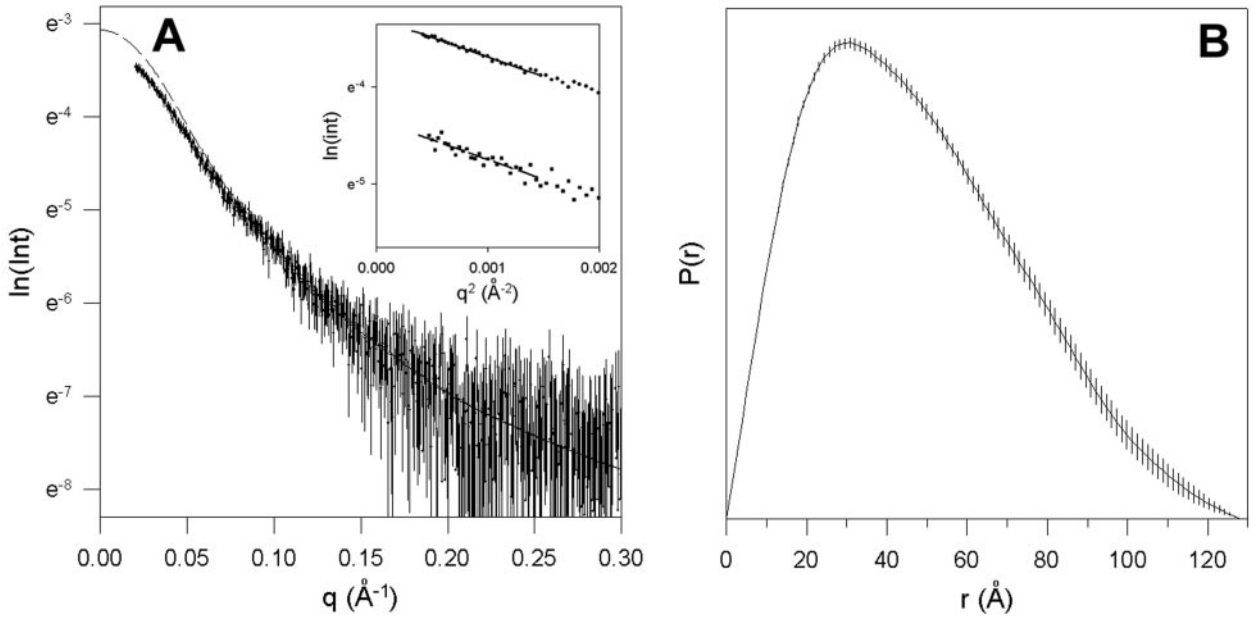

FIGURE 5 (*A*) Small-angle x-ray scattering data and GNOM curve-fitting for a 2.6 mg/ml sAPPα_{695} solution in 50 mM Tris-Cl, pH 7.4. *Points and error bars:* experimental data. *Solid line:* GNOM smeared fit. *Broken line:* GNOM desmeared fit. *Inset:* Guinier diagram of SAXS data. *Upper line*: 2.6 mg/ml sAPPα_{695}. *Lower line*: ~1:2 dilution. Linear fits of data in the validity region of Guinier's law ($R_g \times q \lesssim 1$) yield R_g estimates of 34.8 Å (2.6 mg/ml) and 35 Å (1:2 dilution), showing that concentration-dependent effects do not influence the R_g. (*B*) Pair-distance distribution function for sAPPα_{695}. *Solid line:* calculated from the desmeared GNOM fit shown in panel *A. Error bars:* propagated from experimental error.

detectable dependence of R_g on protein concentration for one additional diluted sample (Fig. 5 *A, inset*). This confirmed the absence of protein concentration dependence on the experimental curve used for subsequent data analysis.

Curve-fitting of the experimental data was performed using the GNOM software package (Svergun and Stuhrmann, 1991). Because our samples proved to be non-interacting dilute systems, the extrapolated value of scattering intensity at zero scattering angle, $I(0)$, was used to obtain an estimate of the molecular weight of sAPPα_{695} in solution, using the relation:

$$MW_{\mathrm{APP}} = \frac{I(0)_{\mathrm{APP}}/c_{\mathrm{APP}}}{I(0)_{\mathrm{Lys}}/c_{\mathrm{Lys}}} \cdot MW_{\mathrm{Lys}} \qquad (4)$$

where c_{Lys} and c_{APP} are, respectively, the concentrations (mg/ml) of a known reference lysozyme sample and of the sAPP sample, calculated from the molar sAPP concentration measured by its absorption band at 280 nm. $I(0)_{\mathrm{Lys}}$ is the zero-angle intensity of the lysozyme sample calculated from a scattering profile measured under exactly the same experimental conditions as sAPPα_{695}, and MW_{Lys} is the molecular weight of lysozyme. The molecular weight of sAPPα_{695} thus calculated was ~62 kDa. In addition, the molecular weight of sAPPα_{695} was also calculated from SAXS data using the scattering intensity of water as a reference, as described by Orthaber et al. (2000). Using this method, sAPPα_{695} was determined to be ~65 kDa. Considering the independent nature of the two methods used for determination of the molecular weight of sAPPα_{695} (i.e., lysozyme versus water as references), the two molecular weight estimates are in excellent agreement. These values are also in good agreement with the calculated polypeptide mass of sAPPα_{695} (69 kDa) plus the invariant N-glycan mass of 2 kDa and some contribution from phosphorylation, sulfation, and O-glycosylation (Weidemann et al., 1989). Calculation of the molecular mass of pure sAPPα_{695} from its relative mobility in SDS-PAGE yielded an estimate of 75 kDa (Fig. 1 *A, lane 4*), which is known to be somewhat higher than the actual molecular weight (Bush et al., 1994). The most important conclusion from the molecular weight estimate is that sAPPα_{695} is undoubtedly a monomer in solution even at 2.6 mg/ml. Furthermore, the volume of the sAPPα_{695} particle was calculated as 81,300 Å^3. This is 5.9 times the volume of the N-terminal fragment (Rossjohn et al., 1999), as calculated from the crystal data including a 3 Å water layer (Svergun et al., 1995). As the polypeptide molecular mass of sAPPα_{695} is 5.7 times the mass of the N-terminal fragment, the close proportionality between molecular volume and mass confirms the validity of the data treatment used and lends further support to the conclusion that sAPPα_{695} is monomeric in solution.

The value of the radius of gyration of sAPPα_{695} obtained from the GNOM fit (Fig. 5 *A*) was 37.9 ± 0.8 Å. This value is in good agreement with the value obtained using the Guinier approximation. The pair-distance distribution func-

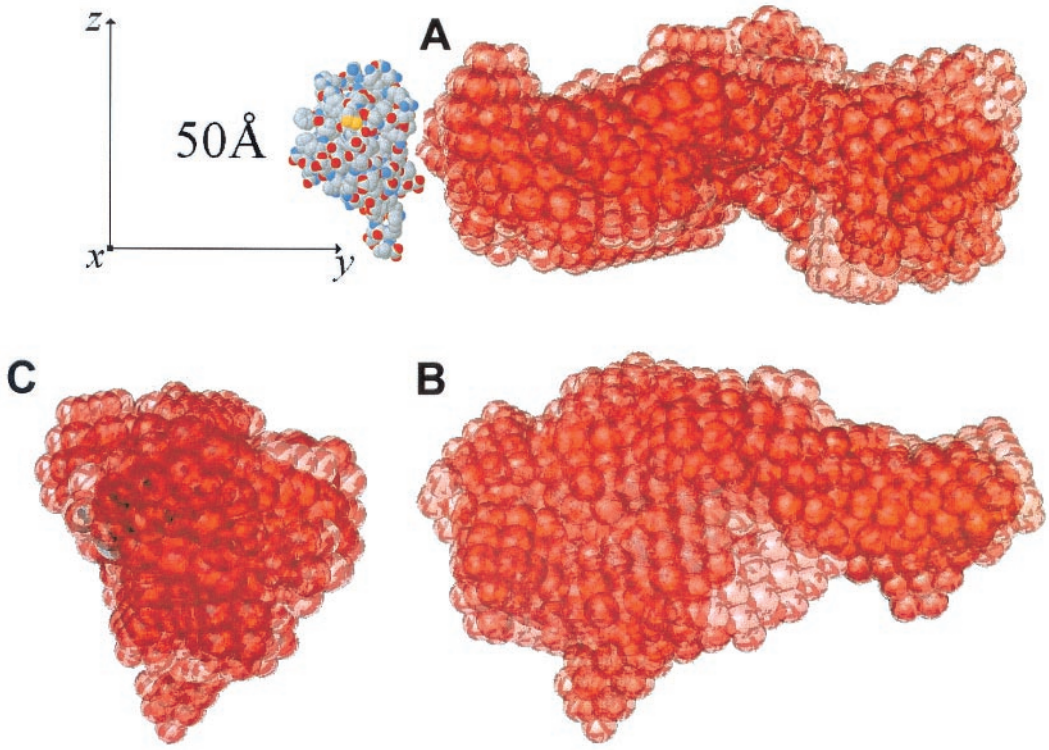

FIGURE 6 (*A–C*) Six superimposed bead model representations of the structural models of sAPPα_{695} calculated using DAMMIN. Panels *B* and *C* are rotated by 90° around the *y* and *z* axis, respectively. The intensity of color indicates the degree of coincidence between the six models. For comparison, the crystal structure of the N-terminal domain of APP (Rossjohn et al., 1999, 1MWP.PDB) is shown in the same scale as panels *A–C*.

tion $P(r)$, shown in Fig. 5 *B*, was calculated from the GNOM fitted data. This curve provided information on another important structural parameter of sAPPα_{695}: the maximum dimension D_{max} = 130 Å, determined from the value of r for which the function $P(r)$ drops to zero. The ratio of the radius of gyration to the maximum dimension indicates an elongated shape for sAPPα_{695} in solution. This is also indicated by the shape of the $P(r)$ function, typical of an anisometric particle (Glatter and Kratky, 1982).

The information content of a SAXS scattering curve is limited by the number of Shannon channels, $N_s = D_{max}(q_{max} - q_{min})/\pi$ (Svergun, 1999). For our measurements on sAPPα_{695}, N_s = 12. The relatively low protein concentration we have used (2.6 mg/ml, equivalent to 41.6 μM sAPPα_{695}) leads to lower precision at high q values. To assess the reliability of the analysis of SAXS data, we performed control measurements for lysozyme as a standard protein under exactly the same conditions utilized for sAPP. Analysis of such data yielded R_g and D_{max} values of 14.4 ± 0.3 Å and 40 ± 5 Å, respectively, for lysozyme (data not shown). These values are in excellent agreement with the well-known dimensions of lysozyme, indicating the reliability of our measurements and methods of analysis.

To obtain a structural model for sAPP in solution, a model-independent calculation based on spherical harmonics was performed using the program SASHA (Svergun et al., 1996). In this calculation, it is assumed that the scattering is caused by globular, homogeneous molecules, and that the molecular envelope function can be approximated by a series of spherical harmonics (Stuhrmann, 1970). The resolution is determined by the maximum number of harmonics used. A rough approximation to the molecular envelope was initially obtained by fitting the q region between 0.02043 Å^{-1} and 0.12 Å^{-1} (~4 Shannon channels). The 3D shape obtained for this low-resolution initial model (not shown) corresponded to an elongated particle, confirming the information provided by the $P(r)$ function. No specific symmetry could be detected from this calculation. The next step for determination of the 3D structure was shape restoration using finite elements (bead models), without symmetry constraints, and simulated annealing optimization. This was performed using the whole range of q measured (12 Shannon channels) and the program DAMMIN (Svergun, 1999) in slow mode, to improve convergence of the simulated annealing procedure to reach a global minimum. Fig. 6 shows the best superimposition (Kozin and Svergun, 2001) of six models obtained from independent calculations. An asymmetric molecular shape was obtained in the analysis. Some parts of the structure agree closely in all six calculations, while other parts are less well-defined. Stokes

TABLE 1 Dimensional data for sAPPα_{695}

Source	R_g (Å)	R_S (Å)	D_{max} (Å)
Gel-filtration data	—	51	—
SAXS data (Guinier)	35	—	—
SAXS data (whole range)	38*	39[†]	130*
Spherical model	24[‡]	31[§]	62[§]

Comparison of radius of gyration (R_g), Stokes radius (R_S), and maximum dimension (D_{max}) determined from experimental data or assuming a spherical model.

*Calculated from the GNOM fit of the SAXS data (Svergun and Stuhrmann, 1991).

[†]Calculated from the DAMMIN model (Svergun, 1999) using HYDRO (Garcia de la Torre, 1994).

[‡]Calculated as $R_g = 2.9 \cdot n^{1.3}$, with n (number of amino acid residues) = 595 for sAPPα_{695} (Gast et al., 1995).

[§]Calculated using $R_S = (5/3)^{1/2} \cdot R_g$ (Luzzati et al., 1961) and $D_{max} = 2 \times R_S$ for spherical molecules.

radii were also calculated for the six models of sAPPα_{695} mentioned above. The calculations were performed using HYDRO (Garcia de la Torre, 1999), yielding a Stokes radius of 38.5 ± 0.1 Å.

DISCUSSION

This study presents, for the first time, a structural model of the extracellular domain of the human amyloid precursor protein in aqueous solution. The secreted extracellular domain of APP (sAPP) shows various biological activities in vivo. On the one hand, sAPP promotes cell growth (Saitoh et al., 1989) and adhesion (Breen et al., 1991), protection from excitotoxicity (Mattson et al., 1993), increase in synaptic density (Roch et al., 1994), and memory consolidation (Meziane et al., 1998). On the other hand, sAPP also activates microglia (Barger and Harmon, 1997) and leads to neuronal damage (Barger and Basile, 2001). It is thought that, as part of the integral transmembrane APP, its extracellular domain mediates similar roles and also stimulates neurite outgrowth (Qiu et al., 1995). Furthermore, sAPP reduces Cu(II) to Cu(I) in vitro (Multhaup et al., 1996) and initiates a Fenton reaction (Multhaup et al., 1998), suggesting a possible role in free radical metabolism. Obtaining a structural model for sAPP and APP may represent an important step toward elucidating the molecular basis of interaction with different biological ligands, leading to the variety of biological activities exhibited by this protein.

SAXS results indicated that sAPPα is monomeric in solution. Interestingly, however, size-exclusion chromatography data indicated that the Stokes radius of sAPPα was significantly higher than that expected for a monomer of the molecular weight of APP (Table 1), suggesting that full-length sAPPα is not a compact spherical molecule. Therefore, we conclude that sAPPα exists predominantly as an extended monomer in solution under physiological conditions. Comparison of the available crystal structure of the N-terminal domain of APP with the structural model of full-length sAPPα_{695} derived from SAXS data (Fig. 6) shows the anisometry of the structure of sAPPα_{695}. As the Stokes radii of the three sAPPα isoforms are the same within experimental error (Fig. 4), it seems probable that sAPPα_{751} and sAPPα_{770} are similarly anisometric. Independent of the detailed final shape of the structural model, the anisometry of sAPP is evident from a comparison of the radius of gyration and the maximum dimension obtained for sAPPα_{695} (Table 1). Although protein glycosylation is expected to result in a small increase in particle size, the large discrepancy between the measured r_g value of 38 Å and D_{max} of 130 Å, and the dimensions predicted for sAPPα_{695} according to a spherical model (Table 1), must be due to a highly non-spherical shape of sAPP.

The extended shape of monomeric sAPPα in solution could result from an elongated rigid structure or from a flexible structure, with disordered segments connecting ordered domains, such as the N-terminal one (Luzzati et al., 1961). Thus, the model derived by spherical harmonics and finite element analysis (Fig. 6) could either depict a rigid molecular shape or the ensemble average of conformationally flexible molecules.

Circular dichroism data analysis supports the notion that >30% of the amino acid residues of APP do not participate in standard secondary structure elements in the protein (Fig. 3 *B*). One possible reason for this may be the existence of disordered regions in sAPP. Indeed, analysis of the primary sequence of sAPP suggests that it could contain disordered segments. A stretch of amino acid residues from 190 to 264 [indicated as $(DE)_n$ in Fig. 1) is strongly negative, with 56% of the residues consisting of Glu and Asp and up to eight contiguous acidic amino acid residues. This region would be difficult to accommodate in an ordered, folded structure. This is one of the two regions without strong homology between APP and the APP-like proteins (APLPs) (Fig. 7; Wasco et al., 1992, 1993). The consensus of the secondary structure prediction algorithms we have used predicts a low content of α-helix and β-sheet in this part of APP (Fig. 7). Second, the two extracellular phosphorylation sites of APP lie in the same region (Caporaso et al., 1992), contributing additional negative charges. The saccharide side chains of APP are also negatively charged (Weidemann et al., 1989) and may therefore exert repulsive interactions upon each other and upon negatively charged regions of the polypeptide chain. Finally, a stretch of amino acid residues that lies upstream from the amyloidogenic Aβ sequence (residues 582 to 663 in APP$_{770}$; labeled RC in Fig. 1) is predicted by 10 different secondary structure prediction algorithms to be devoid of helical or extended sheet structure (Fig. 7). This is the second large region of APP without homology to the otherwise very similar APP-like proteins (APLPs) (see Fig. 7) and therefore may correspond to an important domain for biological functions specifically carried out by APP (see below).

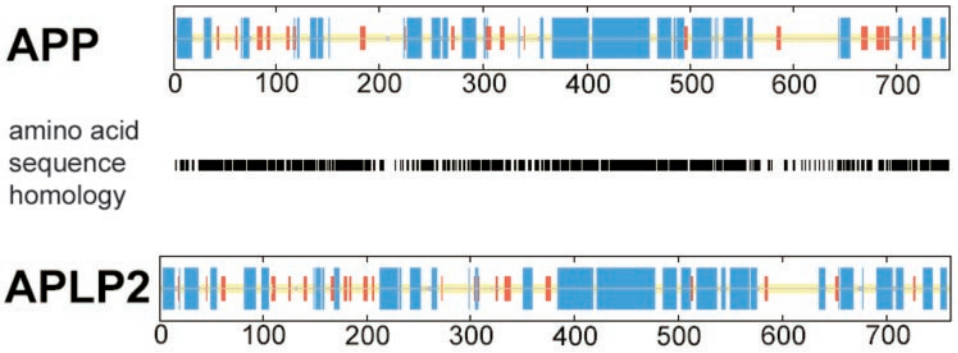

FIGURE 7 Secondary structure prediction and sequence conservation for APP protein family members. The consensus of the secondary structure prediction algorithms (Combet et al., 2000 is shown color-coded for the sequence of APP_{751} (*top diagram*) and its nearest homolog, $APLP2_{763}$ (*bottom diagram*). *Blue bars:* α-helix; *red bars:* β-sheet; *yellow bars:* no secondary structure (random coil); *gray bars:* no consensus. The difference in sequence length is mainly due to a longer signal peptide in APLP2. Amino acid sequence homology between APP and APLP2 (*middle diagram*) is shown as a black bar for each identical or strongly similar residue, according to the CLUSTAL W algorithm implemented in NPS@ (Combet et al., 2000). The sequence marked RC in Fig. 1 corresponds to residues 563 to 644 in APP_{751} (this figure).

Although a stabilizing function for Zn^{2+} ions has been hypothesized (Bush et al., 1994), it is remarkable that the polypeptide crystallized from a solution of APP1-324 (Rossjohn et al., 1999) appeared to contain neither the Cu^{2+} nor the Zn^{2+} binding domains (indicated as CuBD and ZnBD in Fig. 1). This may be analogous to the flexibility of the Cu^{2+} binding site present in the octarepeat Cu^{2+}-binding region of the prion protein (Aronoff-Spencer et al., 2000), which was not resolved in nuclear magnetic resonance structures of the whole prion protein (Donne et al., 1997). In addition to the possible presence of flexible segments in its extracellular domain, the short cytoplasmic domain of APP has been shown by nuclear magnetic resonance studies to be highly mobile (Ramelot et al., 2000). It was hypothesized that this mobility enables APP to bind, at overlapping binding sites, different intracellular ligands with different binding requirements.

Recently, it has become clear that partially unstructured proteins are by no means an exception in the human genome. An unordered structure in the absence of ligand may enable a protein domain to recognize its ligand or multiple ligands with high specificity (Wright and Dyson, 1999). The various extracellular matrix components that bind to sAPP (Narindrasorasak et al., 1992; Beher et al., 1996; Mok et al., 1997; Ohsawa et al., 2001) may well bind alternately to neighboring binding sites.

Another consideration pertinent to the possible flexibility of sAPP is in connection with the lability of this protein in vivo (Koo et al., 1996). The extremely potent memory-affecting (Roch et al., 1994), radical-generating (Multhaup et al., 1998), and cytotoxic (Barger and Basile, 2001) activities of sAPP certainly require precise spatiotemporal mechanisms of regulation (Lyckman et al., 1998) that may involve inhibition and/or degradation of APP. It may be easier to rapidly degrade a flexible protein. Once again, the flexible cytoplasmic domain of APP provides an interesting analogy. After cleavage by γ-secretase, it is released from the plasma membrane into the cytoplasm and is rapidly degraded when not bound to a signal transduction protein (Kimberly et al., 2001). Finally, a flexible structure of sAPP might explain the difficulties in finding the sAPP "receptor" and in elucidating the complete APP signal transduction chain from the extracellular signal to the nucleus (Gao and Pimplikar, 2001; Sisodia and Gallagher, 1998). Our proposed model for the structure of sAPP thus serves as a first step toward elucidation of the transient and alternate molecular interactions of APP with different biological ligands in the extracellular medium.

A further perspective is provided by the fact that a large part of the sequence of sAPP is shared by its homologs APLP1 and APLP2. APP, APLP1, and APLP2 are believed to have similar roles in neurite outgrowth and synapse development (Cappai et al., 1999; Heber et al., 2000) and APP-knockout mice are viable as long as they have a functional APLP1 or APLP2 gene (Heber et al., 2000), probably reflecting the conservation of most domains among all three proteins. However, several neurological deficits and morphological abnormalities have been described in APP-knockout mice (Heber et al., 2000). This suggests there are functions of APP that cannot be compensated by its homologs, and it would appear reasonable to search for their structural correlates in APP-specific regions, such as the random coil region and the amyloidogenic sequence (Figs. 1 and 7). Surprisingly, APLP2, which shares 50% sequence identity and 69% sequence homology with APP_{751} (Fig. 7), has been shown to interact with a major histocompatibility complex class I molecule in the endoplasmic reticulum (Sester et al., 2000) and to be identical with a DNA-binding protein (Rassoulzadegan et al., 1998). It is challenging to explain how proteins of the same family and with such high sequence homology can interact with ligands of such diverse natures and in such varied

environments, unless a significant degree of structural plasticity is taken into account.

This work was supported by grants from the John Simon Guggenheim Memorial Foundation, Howard Hughes Medical Institute, Conselho Nacional de Desenvolvimento Científico e Tecnológico, Fundação de Amparo à Pesquisa do Estado do Rio de Janeiro, Financiadora de Estudos e Projetos, Fundação de Amparo à Pesquisa do Estado de São Paulo, Laboratório Nacional de Luz Síncrotron, and Programa de Apoio ao Desenvolvimento Científico e Tecnológico. S.T.F. is a Howard Hughes Medical Institute International Scholar. M.G. is the recipient of a fellowship from Coordenação de Aperfeiçoamento de Pessoal de Nível Superior.

REFERENCES

Aronoff-Spencer, E., C. S. Burns, N. I. Avdievich, G. J. Gerfen, J. Peisach, W. E. Antholine, H. L. Ball, F. E. Cohen, S. B. Prusiner, and G. L. Millhauser. 2000. Identification of the Cu^{2+} binding sites in the N-terminal domain of the prion protein by EPR and CD spectroscopy. *Biochemistry*. 39:13760–13771.

Barger, S. W., and A. S. Basile. 2001. Activation of microglia by secreted amyloid precursor protein evokes release of glutamate by cystine exchange and attenuates synaptic function. *J. Neurochem.* 76:846–854.

Barger, S. W., and A. D. Harmon. 1997. Microglial activation by Alzheimer amyloid precursor protein and modulation by apolipoprotein E. *Nature.* 388:878–881.

Beher, D., L. Hesse, C. L. Masters, and G. Multhaup. 1996. Regulation of APP binding to collagen and mapping of the binding sites on APP and collagen type I. *J. Biol. Chem.* 271:1613–1620.

Breen, K. C., M. Bruce, and, B. H. Anderton. 1991. Beta-amyloid precursor protein mediates neuronal cell-cell and cell-surface adhesion. *J. Neurosci. Res.* 28:90–100.

Bush, A. I., W. H. Pettingell, M. de Paradis, R. E. Tanzi, and W. Wasco. 1994. The amyloid beta-precursor protein and its mammalian homologues: evidence for a zinc-modulated heparin-binding superfamily. *J. Biol. Chem.* 269:26618–26621.

Caporaso, G. L., S. E. Gandy. J. D. Buxbaum. J. V. Ramabhadran, and P. Greengard. 1992. Protein phosphorylation regulates secretion of Alzheimer beta/A4 amyloid precursor protein. *Proc. Natl. Acad. Sci. U.S.A.* 89:3055–3059.

Cappai, R., S. S. Mok, D. Galatis, D. F. Tucker, A. Henry, K. Beyreuther, D. H. Small, and C. L. Masters. 1999. Recombinant human amyloid precursor-like protein 2 (APLP2) expressed in the yeast *Pichia pastoris* can stimulate neurite outgrowth. *FEBS Lett.* 442:95–98.

Chacón, P., F. Morán, J. F. Díaz, E. Pantos, and J. M. Andreu. 1998. Low-resolution structures of proteins in solution retrieved from x-ray scattering with a genetic algorithm. *Biophys. J.* 74:2760–2774.

Combet, C., C. Blanchet, C. Geourjon, and G. Deléage. 2000. NPS@: Network protein sequence analysis. *Trends Biochem. Sci*. 25:147–150.

De La Fournière-Bessoueille, L., D. Grange, and R. Buchet. 1997. Purification and spectroscopic characterization of beta-amyloid precursor protein from porcine brains. *Eur. J. Biochem.* 250:705–711.

De Strooper, B., and W. Annaert. 2000. Proteolytic processing and cell biological functions of the amyloid precursor protein. *J. Cell Sci.* 113: 1857–1870.

Donne, D. G., J. H. Viles, D. Groth, I. Mehlhorn, T. L. James, F. E. Cohen, S. B. Prusiner, P. E. Wright, and H. J. Dyson. 1997. Structure of the recombinant full-length hamster prion protein PrP(29–231): the N terminus is highly flexible. *Proc. Natl. Acad. Sci. U.S.A.* 94:13452–13457.

Durkin, J. T., S. Murthy, E. J. Husten, S. P. Trusko, M. J. Savage, D. P. Rotella, B. D. Greenberg, and R. Siman. 1999. Rank-order of potencies for inhibition of the secretion of Abeta40 and Abeta42 suggests that both are generated by a single gamma-secretase. *J. Biol. Chem.* 274: 20499–20504.

Gao, Y., and S. W. Pimplikar. 2001. The γ-secretase-cleaved C-terminal fragment of amyloid precursor protein mediates signaling to the nucleus. *Proc. Natl. Acad. Sci. U.S.A.* 98:14979–14984.

Garcia de la Torre, J. 1999. HYDRO: a computer program for the prediction of hydrodynamic properties of macromolecules. *Biophys. J.* 67: 530–531.

Gast, K., H. Damaschun, K. Eckert, K. Schulze-Forster, H. R. Maurer, M. Muller-Frohne, D. Zirwer, J. Czarnecki, and G. Damaschun. 1995. Prothymosin alpha: a biologically active protein with random coil formation. *Biochemistry*. 34:13211–13218.

Glatter, O., and O. Kratky. 1982. Small-Angle X-Ray Scattering. Academic Press, London-New York.

Guinier, A., and G. Fournet. 1955. Small Angle X-Ray Scattering. John Wiley and Sons, New York.

Haass, C., E. H. Koo, D. B. Teplow, and D. J. Selkoe. 1994. Polarized secretion of beta-amyloid precursor protein and amyloid beta-peptide in MDCK cells. *Proc. Natl. Acad. Sci. U.S.A.* 91:1564–1568.

Heber, S., J. Herms, V. Gajic, J. Hainfellner, A. Aguzzi, T. Rulicke, H. von Kretzschmar, C. von Koch, S. Sisodia, P. Tremml, H. P. Lipp, D. P. Wolfer, and U. Müller. 2000. Mice with combined gene knock-outs reveal essential and partially redundant functions of amyloid precursor protein family members. *J. Neurosci.* 20:7951–7963.

Henry, A., C. L. Masters, K. Beyreuther, and R. Cappai. 1997. Expression of human amyloid precursor protein ectodomains in *Pichia pastoris:* analysis of culture conditions, purification, and characterization. *Protein Expr. and Purific.* 10:283–291.

Hesse, L., D. Beher, C. L. Masters, and G. Multhaup. 1994. The beta/A4 amyloid precursor protein binding to copper. *FEBS Lett.* 349:109–116.

Hussain, I., D. Powell, D. R. Howlett, D. G. Tew, T. D. Meek, C. Chapman, I. S. Gloger, K. E. Murphy, C. D. Southan, D. M. Ryan, T. S. Smith, D. L. Simmonds, F. S. Walsh, C. Dingwall, and G. Christie. 1999. Identification of a novel aspartic protease (Asp 2) as beta-secretase. *Mol. Cell. Neurosci.* 14:419–427.

Hynes, T. R., M. Randal, L. A. Kennedy, C. Eigenbrot, and A. A. Kossiakoff. 1990. X-ray crystal structure of the protease inhibitor domain of Alzheimer's amyloid beta-protein precursor. *Biochemistry*. 29: 10018–10022.

Kang, J., H.-G. Lemaire, A. Unterbeck, J. M. Salbaum, C. L. Masters, K.-H. Grzeschik, G. Multhaup, K. Beyreuther, and B. Muller-Hill. 1987. The precursor of Alzheimer's disease amyloid A4 protein resembles a cell-surface receptor. *Nature.* 325:733–736.

Kellermann, G., F. Vicentin, E. Tamura, M. Rocha, H. Tolentino, A. Barbosa, A. Craievich, and I. Torriani. 1997. The small-angle x-ray scattering beamline of the Brazilian Synchrotron Light Laboratory. *J. Appl. Crystallogr.* 30:880–883.

Kimberly, W. T., J. B. Zheng, S. Guenette, and D. J. Selkoe. 2001. The intracellular domain of the beta-amyloid precursor protein is stabilized by Fe65 and translocates to the nucleus in a Notch-like manner. *J. Biol. Chem.* 276:40288–40292.

Kitaguchi, N., Y. Takahashi, Y. Tokushima, S. Shiojiri, and H. Ito. 1988. Novel precursor of Alzheimer's disease amyloid protein shows protease inhibitory activity. *Nature.* 331:530–532.

Kneller, D. G., F. E. Cohen, and R. Langridge. 1990. Improvements in protein secondary structure prediction by an enhanced neural network. *J. Mol. Biol.* 214:171–182.

Koo, E. H., S. L. Squazzo, D. J. Selkoe, and C. H. Koo. 1996. Trafficking of cell-surface amyloid beta-protein precursor. I. Secretion, endocytosis and recycling as detected by labeled monoclonal antibody. *J. Cell Sci.* 109:991–998.

Kozin, M. B., and D. I. Svergun. 2001. Automated matching of high- and low-resolution structural models. *J. Appl. Crystallogr.* 34:33–41.

Laemmli, U. K. 1970. Cleavage of structured proteins during assembly of head of bacteriophage T4. *Nature.* 227:680–685.

Lammich, S., E. Koiro, R. Postina, S. Gilbert, R. Pfeiffer, M. Jasionowski, C. Haass, and F. Fahrenholz. 1999. Constitutive and regulated alpha-secretase cleavage of Alzheimer's amyloid precursor protein by a disintegrin metalloprotease. *Proc. Natl. Acad. Sci. U.S.A.* 96:3922–3927.

Lin, X., G. Koelsch, S. Wu, D. Downs, A. Dashti, and J. Tang. 1999. Human aspartic protease memapsin 2 cleaves the beta-secretase site of beta-amyloid precursor protein. *Proc. Natl. Acad. Sci. U.S.A.* 97: 1456–1460.

Luzzati, V., J. Witz, and A. Nicolaieff. 1961. La structure de la sérum albumine de boeuf en solution à pH 5.3 e 3.6: étude par diffusion central absolue de rayons X. *J. Mol. Biol.* 3:379–392.

Lyckman, A. W., A. M. Confaloni, G. Thinakaran, S. S. Sisodia, and K. L. Moya. 1998. Post-translational processing and turnover kinetics of presynaptically targeted amyloid precursor superfamily proteins in the central nervous system. *J. Biol. Chem.* 273:11100–11106.

Masters, C. L., G. Simms, N. A. Weinman, G. Multhaup, B. L. McDonald, and K. Beyreuther. 1985. Amyloid plaque core protein in Alzheimer disease and Down syndrome. *Proc. Natl. Acad. Sci. U.S.A.* 82: 4245–4249.

Mattson, M., B. Cheng, A. R. Culwell, F. S. Esch, I. Liebersburg, and R. E. Rydel. 1993. Evidence for excitoprotective and intraneuronal calcium-regulating roles for secreted forms of the beta-amyloid precursor protein. *Neuron.* 10:243–254.

Meziane, H., J.-C. Dodart, C. Mathis, S. Little, J. Clemens, S. M. Paul, and A. Ungerer. 1998. Memory-enhancing effects of secreted forms of the beta-amyloid precursor protein in normal and amnestic mice. *Proc. Natl. Acad. Sci. U.S.A.* 95:12683–12688.

Mok, S. S., G. Sberna, D. Heffernan, R. Cappai, D. Galatis, H. J. Clarris, W. H. Sawyer, K. Beyreuther, C. L. Masters and, D. H. Small. 1997. Expression and analysis of heparin-binding regions of the amyloid precursor protein of Alzheimer's disease. *FEBS Lett.* 415:303–307.

Multhaup, G., T. Ruppert, A. Schlicksupp, L. Hesse, E. Bill, R. Pipkorn, C. L. Masters, and K. Beyreuther. 1998. Copper-binding amyloid precursor protein undergoes a site-specific fragmentation in the reduction of hydrogen peroxide. *Biochemistry.* 37:7224–7230.

Multhaup, G., A. Schlicksupp, L. Hesse, D. Beher, T. Ruppert, C. L. Masters, and K. Beyreuther. 1996. The amyloid precursor protein of Alzheimer's disease in the reduction of copper(II) to copper(I). *Science.* 271:1406–1409.

Narindrasorasak, S., D. E. Lowery, R. A. Altman, P. A. Gonzalez-De Whitt, B. D. Greenberg, and R. Kisilevsky. 1992. Characterization of high-affinity binding between laminin and Alzheimer's disease amyloid precursor proteins. *Lab. Invest.* 67:643–652.

Ohsawa, I., C. Takamura, and S. Kohsaka. 2001. Fibulin-1 binds the amino-terminal head of beta-amyloid precursor protein and modulates its physiological function. *J. Neurochem.* 76:1411–1420.

Oliveira, C. L. P., D. R. dos Santos, G. Kellermann, T. Plivelic, and I. L. Torriani. 1997. Data treatment program for the SAXS Beamline. LNLS Technical Note, Laboratorio Nacional de Luz Sincrotron, Campinas, Brazil.

Orthaber, D., A. Bergmann, and O. Glatter. 2000. SAXS experiments on absolute scale with Kratky systems using water as a secondary standard. *J. Appl. Crystallogr.* 33:218–225.

Pace, C. N., F. Vajdos, L. Fee, G. Grimsley, and T. Gray. 1995. How to measure and predict the molar absorption coefficient of a protein. *Protein Sci.* 4:2411–2423.

Ponte, P., P. Gonzalez-De Whitt, J. Schilling, J. Miller, D. Hsu, and B. Greenberg. 1988. A new A4 amyloid mRNA contains a domain homologous to serine protease inhibitors. *Nature.* 331:525–527.

Proudfoot, J. M., K. D. Croft, I. B. Puddey, and L. J. Beilin. 1997. The role of copper reduction by alpha-tocopherol in low-density lipoprotein oxidation. *Free Radic. Biol. Med.* 23:720–728.

Qiu, W. Q., A. Ferreira, C. Miller, E. H. Koo, and D. J. Selkoe. 1995. Cell-surface beta-amyloid precursor protein stimulates neurite outgrowth of hippocampal neurons in an isoform-dependent manner. *J. Neurosci.* 15:2157–2167.

Ramelot, T. A., L. N. Gentile, and L. K. Nicholson. 2000. Transient structure of the APP cytoplasmic tail indicates preordering of structure for binding to cytosolic factors. *Biochemistry.* 39:2714–2725.

Rassoulzadegan, M., Y. Yang, and F. Cuzin. 1998. APLP2, a member of the Alzheimer precursor protein family, is required for correct genomic segregation in dividing mouse cells. *EMBO J.* 17:4647–4656.

Roch, J. M., E. Masliah, A.-C. Roch-Levecq, M. P. Sundsmo, D. A. C. Otero, I. Veinbergs, and T. Saitoh. 1994. Increase of synaptic density and memory retention by a peptide representing the trophic domain of the amyloid beta/A4 protein precursor. *Proc. Natl. Acad. Sci. U.S.A.* 91:7450–7454.

Rossjohn, J., R. Cappai, S. C. Feil, A. Henry, W. J. McKinstry, D. Galatis, L. Hesse, G. Multhaup, K. Beyreuther, C. L. Masters, and M. W. Parker. 1999. Crystal structure of the N-terminal growth factor-like domain of Alzheimer amyloid precursor protein. *Nat. Struct. Biol.* 6:327–331.

Saitoh, T., M. Sundsmo, J. M. Roch, N. Kimura, G. Cole, D. Schubert, T. Oltersdorf, and D. B. Schenk. 1989. Secreted form of amyloid beta protein precursor is involved in the growth regulation of fibroblasts. *Cell.* 58:615–622.

Sester, M., D. Feuerbach, R. Frank, T. Preckel, A. Gutermann, and H.-G. Burgert. 2000. The amyloid precursor-like protein 2 associates with the major histocompatibility complex class I molecule K_d. *J. Biol. Chem.* 275:3645–3654.

Seubert, P., T. Oltersdorf, M. G. Lee, R. Barbour, C. Blomquist, D. L. Davis, K. Bryant, L. C. Fritz, D. Galasko, L. J. Thal, I. Lieberburg, and D. S. Schenk. 1993. Secretion of beta-amyloid precursor protein cleaved at the amino terminus of the beta-amyloid peptide. *Nature.* 361: 260–263.

Siegel, L. M., and K. J. Monty. 1966. Determination of molecular weights and frictional ratios of proteins in impure systems by use of gel filtration and density gradient centrifugation. Application to crude preparations of sulfite and hydroxylamine reductases. *Biochim. Biophys. Acta.* 112: 346–362.

Sinha, S., J. P. Anderson, R. Barbour, G. S. Basi, R. Caccavello, D. Davis, M. Doan, H. F. Dovey, N. Frigon, J. Hong, K. Jacobson-Croak, N. Jewett, P. Keim, J. Knops, I. Lieberburg, M. Power, H. Tan, G. Tatsuno, J. Tung, D. Schenk, P. Seubert, S. M. Suomensaari, S. Wang, D. Walker, J. Zhao, L. McConlogue, and J. Varghese. 1999. Purification and cloning of amyloid precursor protein beta-secretase from human brain. *Nature.* 402:537–540.

Sisodia, S. S., and M. Gallagher. 1998. A role for the beta-amyloid precursor protein in memory? *Proc. Natl. Acad. Sci. U.S.A.* 95: 12074–12076.

Sreerama, N., and R. W. Woody. 2000. Estimation of protein secondary structure from circular dichroism spectra: comparison of CONTIN, SELCON and CDSSTR methods with an expanded reference set. *Anal. Biochem.* 287:252–260.

Stuhrmann, H. B. 1970. Interpretation of small-angle scattering functions of dilute solutions and gases. A representation of the structures related to a one-particle function. *Acta Crystallogr. A.* 26:297.

Svergun, D. I. 1999. Restoring low resolution structure of biological macromolecules from solution scattering using simulated annealing. *Biophys. J.* 76:2879–2886.

Svergun, D. I. 2001. Determination of domain structure of proteins from x-ray solution scattering. *Biophys. J.* 80:2946–2953.

Svergun, D. I., C. Barberato, and, M. H. J. Koch. 1995. CRYSOL: a program to evaluate x-ray solution scattering of biological macromolecules from atomic coordinates. *J. Appl. Crystallogr.* 28:768–773.

Svergun, D. I., and H. B. Stuhrmann. 1991. New developments in direct shape determination from small-angle scattering. 1. Theory and model calculations. *Acta Crystallogr. A.* 47:736–744.

Svergun, D. I., V. V. Volkov, M. B. Kozin, and H. B. Stuhrmann. 1996. New developments in direct shape determination from small-angle scattering. 2. Uniqueness. *Acta Crystallogr. A.* 52:419–426.

Tanzi, R. E., A. J. McClatchy, E. D. Lamperti, L. Villa-Komaroff, J. F. Gusella, and R. L. Neve. 1988. Protease inhibitor domain encoded by an amyloid protein precursor mRNA associated with Alzheimer's disease. *Nature.* 331:528–532.

Trewhella, J. 1997. Insights into biomolecular function from small-angle scattering. *Curr. Opin. Struct. Biol.* 7:702–708.

Van Nostrand, W. E., S. L. Wagner, J. S. Farrow, and D. D. Cunningham. 1990. Immunopurification and protease inhibitory functions of platelet protease nexin-2/amyloid beta-protein precursor. *J. Biol. Chem.* 265: 9591–9594.

Vassar, R., B. D. Bennett, S. Babu-Khan, S. Kahn, E. A. Mendiaz, P. Denis, D. B. Teplow, S. Ross, P. Amarante, R. Loeloff, Y. Luo, S. Fisher, J. Fuller, S. Edenson, J. Lile, M. A. Jarosinski, A. L. Biere, E. Curran, T. Burgess, J. C. Louis, F. Collins, J. Treanor, G. Rogers, and M. Citron. 1999. beta-secretase cleavage of Alzheimer's amyloid precursor protein by the transmembrane aspartic protease BACE. *Science.* 286:735–741.

Wasco, W., K. Bupp, M. Magendantz, J. F. Gusella, R. E. Tanzi, and F. Solomon. 1992. Identification of a mouse brain cDNA that encodes a protein related to the Alzheimer disease-associated amyloid beta protein precursor. *Proc. Natl. Acad. Sci. U.S.A.* 89:10758–10762.

Wasco, W., S. Gurubhagavatula, M. de Paradis, D. Romano, S. S. Sisodia, B. T. Hyman, R. L. Neve, and R. E. Tanzi. 1993. Isolation and characterization of APLP2 encoding a homolog of the Alzheimer's associated amyloid beta protein precursor. *Nature Genet.* 5:95–100.

Weidemann, A., G. König, D. Bunke, P. Fisher, J. M. Salbaum, C. L. Masters, and K. Beyreuther. 1989. Identification, biogenesis and localization of precursors of Alzheimer's disease A4 amyloid protein. *Cell.* 57:115–126.

Wright, P. E., and H. J. Dyson. 1999. Intrinsically unstructured proteins: re-assessing the protein structure-function paradigm. *J. Mol. Biol.* 293: 321–331.

Yan, R., M. J. Bienkowski, M. E. Shuck, H. Miao, M. C. Tory, A. M. Pauley, J. R. Brashler, N. C. Stratman, W. R. Mathews, A. E. Buhl, D. B. Carter, A. G. Tomasselli, L. A. Parodi, R. L. Heinriksson, and M. E. Gurney. 1999. Membrane-anchored aspartyl protease with Alzheimer's disease beta-secretase activity. *Nature.* 402: 533–537.